ACCSCIENCE PUBLISHING

Journal of Chinese Architecture and Urbanism

ORIGINAL ARTICLE

Influence of land use patterns on urban heat island dynamics in an emerging megacity: A case study of Zhengzhou, Henan, China

Emmanuel Yeboah[1], Isaac Sarfo[2,3]*, Clement Kwang[4], Philip Kofi Alimo[5], Michael Atuahene Djan[6], Millicent Selase Afenya[7], Abraham Okrah[8], and Solomon Obiri Yeboah Amankwah[9]

[1]School of Remote Sensing and Geomatics Engineering, Nanjing University of Information Science and Technology, Nanjing, Jiangsu, China

[2]College of Geography and Environmental Science, Henan University, Kaifeng, Henan, China

[3]Organization of African Academic Doctors (OAAD), Nairobi, Kenya

[4]Department of Geography and Resource Development, University of Ghana, Accra, Greater Accra Region, Ghana

[5]College of Transportation Engineering, Tongji University, Shanghai, China

[6]Department of Geography, University of Nebraska, Lincoln, Nebraska, United States of America

[7]School of International Education, Henan Polytechnic, Zhengzhou, Henan, China

[8]Collaborative Innovation Center on Forecast and Evaluation of Meteorological Disaster, Nanjing University of Information Science and Technology, Nanjing, Jiangsu, China

[9]Department of Small Island Sustainability, University of the Bahamas, Nassau, Bahamas

(This article belongs to the *Special Issue: Design of Eco-Cities and Transportation Systems*)

Abstract

This study investigates the influence of land use and land cover change (LULCC) on urban heat island (UHI) effects in Zhengzhou, Henan, China, amid rapid urbanization and significant landscape transformations between 1993 and 2023. Employing remote sensing and geospatial analytical methods, we analyze the spatiotemporal dynamics of UHI intensity and its relationship with LULCC variables, including built-up areas, bare land, farmlands, forests, water bodies, and grasslands/shrubs. Our findings reveal a dramatic increase in UHI intensity, rising from 1.02°C in 1993 to 2.49°C in 2023, closely associated with a 130.78% expansion of built-up areas (from 1,951.13 sqkm to 4,502.84 sqkm). Concurrently, vegetative cover has declined significantly, with forests and farmlands decreasing by 43.37% and 70.90%, respectively. Geodetector analysis stresses the role of built-up areas as the primary driver of UHI, with a strong positive correlation with UHI (R = 0.729). Conversely, farmlands (R = −0.891) and forests (R = −0.962) demonstrate notable negative correlations, highlighting their critical cooling functions. K-means clustering analysis identifies spatial heterogeneity in UHI effects, with densely built-up clusters exhibiting the highest UHI intensities, whereas vegetated and water-dominated clusters exhibit significantly lower values. These findings emphasize the detrimental impact of urbanization on local thermal dynamics while emphasizing the importance of preserving green spaces and water bodies in mitigating UHI effects. Our standpoints drive the urgent need for sustainable land-use policies that integrate green infrastructure into urban planning frameworks. These insights are crucial for fostering climate-resilient cities in the face of ongoing urbanization and climate change.

Keywords: Land use and land cover change; Urban heat islands; Geodetector; Clustering; Urban sprawl; China

***Corresponding author:**
Isaac Sarfo
(isaacsarfo@henu.edu.cn)

Citation: Yeboah, E., Sarfo, I., Kwang, C., Alimo, P.K., Djan, M.A., Afenya, M.S., *et al*. (2026). Influence of land use patterns on urban heat island dynamics in an emerging megacity: A case study of Zhengzhou, Henan, China. *Journal of Chinese Architecture and Urbanism,* 8(1):8412. https://doi.org/10.36922/jcau.8412

Received: January 5, 2025

1st revised: March 9, 2025

2nd revised: April 3, 2025

3rd revised: April 24, 2025

Accepted: April 24, 2025

Published online: May 14, 2025

1. Introduction

Urban growth significantly influences climate, regional atmospheric composition, water and energy equilibrium, urban surface properties, natural resource ecosystems, and temperature fluctuations (Li *et al*., 2022). With projections indicating that 70% of the global population will reside in cities by 2025, and over 55% already living in urban areas as of 2022 (United Nations Statistics Division, 2022), the environmental impacts of urbanization are becoming increasingly pronounced. One of the most notable consequences of urbanization is the urban heat island (UHI) effect, which refers to the phenomenon where urban areas experience significantly higher temperatures compared to their surrounding rural regions. This temperature disparity arises from factors such as the replacement of natural landscapes with heat-absorbing materials (e.g., concrete and asphalt), reduced vegetation, and increased anthropogenic heat emissions (Vujovic *et al*., 2021). The UHI effect not only exacerbates local warming but also influences microclimates, energy consumption, and public health, making it a critical area of study in the context of rapid urbanization and climate change. This tendency, driven by human-induced heat emissions, altered urban structures, and reduced vegetation, intensifies alongside ongoing urbanization and climate change (Kamal *et al*., 2023). The UHI directly affects the microclimate and atmospheric conditions, degrades urban air and water quality, increases summer energy demand, and heightens thermal health risks, thereby contributing to increased morbidity and mortality among urban residents (Li *et al*., 2024). Given the imminent threats to the well-being of the urban inhabitants and the accelerating pace of urbanization, the UHI phenomenon has emerged as a significant environmental concern, especially in highly urbanized countries like China (Tian *et al*., 2021).

China's economic expansion has rendered it one of the world's industrialized and urbanized nations, with the urbanization rate rising from 10.6% in 1984 to 66.2% in 2023 (National Bureau of Statistics, 2024). Sarfo *et al*. (2024) and Li *et al*. (2022) report that UHI effects in Zhengzhou, Henan, China, have markedly intensified due to spatial expansion and increased urbanization heat intensity; the high-temperature area expanded by 138.7 sqkm from 2006 to 2014, with warming occurring at a rate 2.2 times higher than the global land average from 1981 to 2019. These patterns highlight the pressing need to study UHI dynamics in China, especially in light of global warming and the country's carbon neutrality goals, which necessitate innovative mitigation measures (Han *et al*., 2024). China's continuing urbanization is expected to significantly exacerbate the UHI effect, driven by land-use changes and population growth (Zhao *et al*., 2022). Addressing UHI in urban centers is essential to safeguarding public health, reducing energy demands, and improving climate resilience, while providing a theoretical foundation for urban planning and sustainable development. This is critically necessary and carries substantial practical ramifications for enhancing the living conditions of urban inhabitants (Li *et al*., 2024; Sarfo *et al*., 2024).

When Nieuwolt (1966) conducted one of the earliest studies on the impacts of UHI in metropolitan southern Singapore in 1964, it set the stage for future UHI research. Over the years, a number of studies, such as those by Grover & Singh (2015) and Ogashawara and Bastos (2012), have examined the complex nature of UHIs. These studies consistently demonstrate that urban surface temperatures are heavily influenced by variations in built-up areas, aquatic bodies, and vegetation (Grover & Singh, 2015; Sarfo *et al*., 2024). For instance, the proliferation of impermeable surfaces promotes heat absorption, while reduced vegetation diminishes cooling effects, thereby aggravating UHI events (Vujovic *et al*., 2021). Although land use and land cover change (LULCC) are important drivers of urban form, climate conditions also play a significant role in influencing UHI dynamics (Hu *et al*., 2024). As a result, while land cover is crucial for regulating urban temperature, its interconnections with broader socio-environmental systems must be considered to fully explain UHI fluctuations (Wang, 2024).

Studies emphasize that the spatiotemporal dynamics of LULCC are critical in shaping UHI effects, exhibiting variations that are both spatially and temporally significant (Grover & Singh, 2015; Sarfo *et al*., 2024). Alterations in land cover, including urban encroachment into green spaces or the substitution of permeable surfaces with impermeable materials, modify the thermal characteristics of the surface and their heat retention capacities (Wang, 2024). These modifications exacerbate UHI intensity over time, leading communities to encounter higher temperatures as urbanization progresses (Liu *et al*., 2024). Furthermore, temporal fluctuations in UHI intensity, including seasonal or diurnal changes, are affected by varying anthropogenic activities, climatic circumstances, and patterns of LULCCs during specified intervals (Tesfamariam *et al*., 2023). UHI impacts are further shaped by patterns of urban expansion and the dominant types of land cover (Hu *et al*., 2024).

The "urban canyon effect," for instance, describes how dense clusters of high-rise buildings can trap heat by reducing ventilation (Voogt & Oke, 2003). Conversely, areas containing water bodies or green spaces exhibit

cooler microclimates due to their reflective properties and evapotranspiration effects (Han *et al*., 2024). Studies also indicate considerable spatial heterogeneity in UHI intensity across urban areas, highlighting the need for localized modeling methods rather than aggregated models that overlook these discrepancies (Zhao *et al*., 2022). Thus, the UHI effect is a dynamic phenomenon, with intensity fluctuating in response to temporal alterations in land use and spatial variations in urban structure and land cover composition (Vujovic *et al*., 2021).

Over the past few decades, Zhengzhou, a major city in central China, has experienced substantial LULCC alongside rapid economic development (Chen *et al*., 2023; Sarfo *et al*., 2024). The city's designation as a key hub within the Zhongyuan Urban Agglomeration, along with the establishment of the Zhengzhou Airport Economic Experimental Zone, has accelerated urbanization and growth (Mu *et al*., 2016). This rapid urban expansion has led to frequent changes in land use categories, intensifying the interaction between environmental factors, particularly the UHI phenomenon, and urban development (Hu *et al*., 2024). For instance, built-up areas in Zhengzhou expanded by 53.61% between 1993 and 2023, while woodlands, agricultural land, water bodies, grasslands, and unused land decreased by 17.12%, 5.00%, 18.31%, 21.59%, and 94.48%, respectively (Zhao & Miao, 2022). Although these changes have significantly altered Zhengzhou's landscape and influenced UHI dynamics, their specific impacts remain inadequately examined in this context (Cai *et al*., 2022).

Despite extensive research on UHIs, critical gaps persist in understanding their long-term, localized dynamics within rapidly urbanizing cities such as Zhengzhou (Chen *et al*., 2023). Prior studies have predominantly focused on urban agglomerations or single-city snapshots, often overlooking spatial variability and the nuanced impacts of LULCC (Cai *et al*., 2022). Furthermore, the influence of urban functional zones on UHI intensity, particularly under extreme heat conditions, remains understudied (Li *et al*., 2024).

To address these gaps, this study: (i) analyzes three decades (1993 – 2023) of UHI trends in Zhengzhou, Henan, China; (ii) evaluates spatial variations tied to urban expansion and key land cover types; and (iii) assesses how LULCC influence UHI intensity during extreme hot and dry conditions over the same period. By integrating temporal and spatial dimensions, this research offers actionable insights for sustainable urban design, providing planners with evidence-based strategies to mitigate UHI effects, enhance thermal comfort, and reduce heat-related health risks (Chen *et al*., 2023; Li *et al*., 2024). The findings contribute to a transferable framework for UHI management in Zhengzhou and comparable emerging megacities globally.

2. Data and methods

2.1. Description of the study area

Zhengzhou (Figure 1), located in the central plains of China, is the capital city of Henan province. The city's geographical coordinates are approximately 34.7466° N latitude and 113.6254° E longitude. With a population exceeding 10 million, it ranks among the most populous cities in China. Situated along the southern banks of the Yellow River, Zhengzhou serves as an important transportation hub, with several major railway lines converging in the city. Its strategic location has made it a key economic and cultural center in the region. The city experiences a continental monsoon climate, characterized by hot, humid summers and cold, dry winters. Seasonal temperature fluctuations are significant, with summer highs reaching up to 40°C and winter lows falling below freezing.

The climatic pattern exacerbates the UHI effect, particularly during extreme weather events such as heatwaves. Average summer temperatures often exceed 35°C, intensifying the urban thermal environment and increasing vulnerability to heat stress among urban residents. Urban expansion further amplifies UHI dynamics. Zhengzhou features a mix of densely built-up high-rise zones and sprawling peri-urban developments interspersed with green spaces and agricultural lands. This heterogeneity in land cover types and urban structure contributes to spatial variability in UHI intensity, making Zhengzhou a suitable case study for investigating the relationships between LULCC, urban expansion, and microclimatic conditions. In addition, Zhengzhou offers opportunities to explore the effects of urban design and planning strategies on UHI mitigation, particularly given its history of targeted urban renewal and ecological restoration projects (Grover & Singh, 2015).

2.2. Data

This study utilizes 30 Landsat images with a 30-m resolution, from 1993 to 2023, acquired from the United States Geological Survey website (http://earthexplorer.usgs.gov/). Image preprocessing was carried out using ArcGIS 10.8, ENVI versions 5.0 and 5.3. As illustrated in Figure 2, preprocessing involved image calibration, layer stacking, and supervised classification, following the description of classes summarized in Table 1. For classification, specific spectral bands were utilized: Bands 7, 4, and 2 for Landsat 5 TM (1993 – 2001) and Landsat 7 ETM+ (2002 – 2015), and Bands 7, 5, and 3 for Landsat 8 OLI/TIRS (2016 – 2023), with appropriate row/path configurations. In addition, 2-meter land surface temperature (LST) data spanning

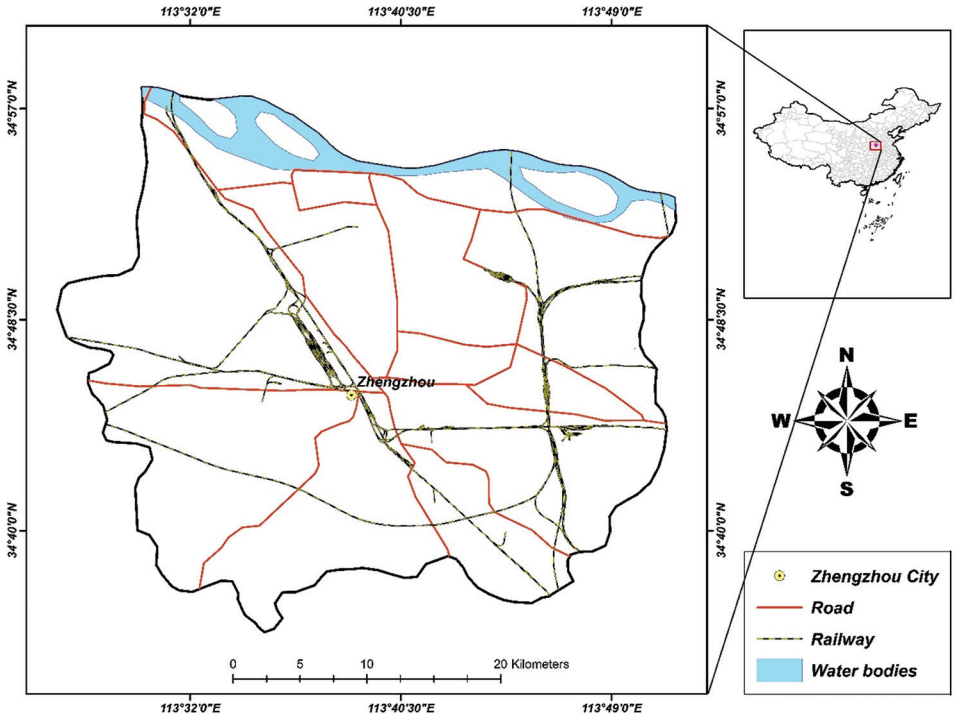

Figure 1. Geographical location of Zhengzhou city in Central China
Source: Map by the authors

the same 30-year period (1993 – 2023) were sourced from the fifth-generation European Centre for Medium-Range Weather Forecasts Reanalysis dataset (ERA5).

2.3. Methods

The methodological flowchart, as presented in Figure 2, is divided into three main stages that structure the analytical process. Each stage is elaborated upon in the subsequent subsections to offer a thorough explanation of the methodology.

2.3.1. Land cover classification and change analysis

Supervised image classification techniques were employed to classify land cover data into six distinct categories: built-up areas, forests, bare land, water bodies, farmlands, grasslands, and shrubs. The classification process utilized the Maximum Likelihood Classification Algorithm (Mishra *et al.*, 2020), which assigns each pixel or spatial unit to a specific land cover class based on spectral signatures and training data using a probabilistic approach.

To assess the accuracy of the land use classifications (Appendix) from 1993 to 2023, ground-truth samples were collected from randomly selected locations and validated using Google Earth Pro. For each land-use class (bare land, built-up, water bodies, forests, farmlands, and grasslands and shrubs), 100 samples were generated from the classified images for each year, resulting in a total of 600 samples per year. Accuracy assessment relied on user accuracy, producer accuracy, and the Kappa coefficient to evaluate and validate the classification results.

To minimize potential classification biases, a rigorous sampling strategy was implemented. Random sampling ensured that the ground-truth points were representative of each land-use class across the study area. These points were cross-verified using Google Earth Pro for visual validation, providing an additional layer of accuracy confirmation. Expert knowledge was also utilized to resolve ambiguities or misclassifications. Furthermore, multiple algorithms and feature selection methods were tested to enhance classification reliability. The combined use of user accuracy, producer accuracy, and the Kappa coefficient ensured a robust and credible assessment of classification performance, minimizing biases and improving the overall quality of the land cover classification.

A change detection analysis was conducted to evaluate land use continuity and identify the driving factors behind these changes in Zhengzhou. The analytical framework was based on the mathematical formulations provided in Equations I, II, and III:

$$\text{Change in LULCC} = \frac{\text{LULCC}_{\text{Current year}} - \text{LULCC}_{\text{Past year}}}{\text{LULCC}_{\text{Past year}}} \quad \text{(I)}$$

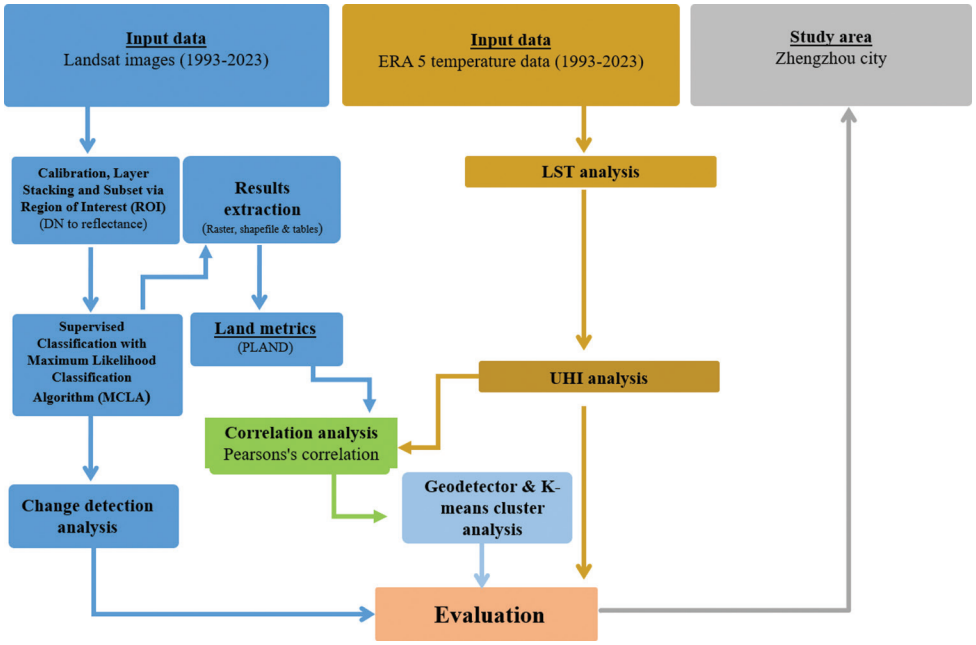

Figure 2. Methodological framework designed for this study
Source: Diagram by the authors
Abbreviations: DN: Digital number; LST: Land surface temperature; UHI: Urban heat island

$$\% \text{ Change in LULCC} = \frac{\text{LULCC}_{\text{Current year}} - \text{LULCC}_{\text{Past year}}}{\text{LULCC}_{\text{Past year}}} \times 100 \quad \text{(II)}$$

$$\text{Rate of change in LULCC per year} = \left[\left(\frac{\text{LULCC}_{\text{Current year}} - \text{LULCC}_{\text{Past year}}}{\text{LULCC}_{\text{Past year}}} \right) \times 100\% \right] \div 30 \text{ years} \quad \text{(III)}$$

2.3.2. LST and UHI analyses

The UHI effect was quantified by measuring LST across different regions of Zhengzhou city and comparing urban temperatures to those of surrounding rural areas. The analytical framework relied on the mathematical Equations IV and V:

$$\text{LST} = \left(\frac{K_2}{\ln\left(\frac{K_1}{\text{Radiance} + K_0} + 1 \right)} \right) - 273.15 \quad \text{(IV)}$$

Where:

- LST is the land surface temperature in degrees Celsius (°C)
- Radiance is the radiance observed by the sensor
- K_0, K_1, and K_2 are sensor-specific calibration constants.

The LST maps were derived from Landsat imagery with a 30-m spatial resolution, offering a balance between regional-scale analysis and computational efficiency. While this resolution effectively captures broad temperature patterns, such as urban–rural contrasts, it may not fully resolve fine-scale heterogeneity caused by variations in building density, vegetation, or surface materials. Interpolation techniques were applied to ensure continuous coverage and coherent visualization of LST patterns across the study area.

$$\text{UHI} = \text{LST}_{\text{urban}} - \text{LST}_{\text{rural}} \quad \text{(V)}$$

Where:

- *UHI* is the urban heat island
- LST_{urban} is the land surface temperature in the urban area
- LST_{rural} is the land surface temperature in the rural (non-urban) area.

2.4. Land metric and UHI analysis

Supervised image classification techniques were used to categorize land cover data into various classes. Each pixel was assigned to a specific land cover type. Land

Table 1. Description of classes used in this study

Feature	Definition
Forests	Densely vegetated areas with intertwined tree canopies and no exposed soil.
Built-up	Encompasses urban, commercial, and industrial zones, as well as community green spaces, sports fields, and truck terminals.
Bare land	Uncovered areas consisting of soil or rocks with little or no vegetation, often observed in cleared and underdeveloped areas.
Farmlands	Agricultural zones, including cultivated fields, orchards, and rural plots used for crop production.
Water bodies	Natural and artificial water features such as rivers, lagoons, lakes, and reservoirs.
Grasslands and shrubs	Areas dominated by trees, hedges, bushes, secluded thickets, and grasses, forming a patchy mosaic of vegetation.

metrics were calculated using the percentage of landscape (PLAND).

$$PLAND = 100 \times \sum_{x=a_{jm}}^{n} /T \quad \text{(VI)}$$

Where n is the number of patches in the landscape for class x; a_{jm} is the area of patch jm; T is the total landscape area.

This metric represents the proportion of the total area occupied by a particular land-use type. It provides valuable insights into the spatial distribution and configuration of land cover types within a defined area.

To explore the relationship between PLAND and UHI intensity, we performed a statistical analysis utilizing correlation techniques. Specifically, we examined how changes in PLAND values for specific land use classes corresponded to variations in UHI intensity across the study area. Pearson correlation coefficients were calculated to quantify the strength and direction of these relationships:

$$R = \frac{\sum(m_i - \mu)(n_i - \delta)}{\sqrt{\sum(m_i - \mu)^2 \sum(n_i - \delta)^2}} \quad \text{(VII)}$$

Where:

- R = Correlation coefficient
- m_i = Values of the x-variable in the sample
- μ = Average values of the x-variable
- n_i = Values of the y-variable in the sample
- δ = Average values of the y-variable.

A correlation heatmap was also generated to visualize the relationships between multiple variables in the dataset. This heatmap presents a visual representation of the correlation coefficients (R) between pairs of variables, facilitating the identification of patterns, trends, and dependencies. Positive correlations (values close to 1) indicate that two variables tend to increase or decrease simultaneously, while negative correlations (values close to −1) indicate an inverse relationship.

2.5. Geodetector and K-means clustering analysis

Geodetector (http://www.geodetector.cn/) is a statistical tool designed to quantify the spatial association between LULCC features and UHI variations. Its significance lies in its ability to identify and measure the impact of specific land cover classes on UHI spatial patterns, providing a robust framework for uncovering the drivers of urban heat dynamics and informing targeted mitigation strategies (Wang *et al.*, 2021).

In this study, we utilized q-statistics within the Geodetector framework to quantify spatial heterogeneity and identify the dominant factors influencing UHI variations (Equation VIII):

$$q = \frac{\sum_{a=1}^{L} Na^{\sigma_a^2}}{N^{\sigma^2}} \quad \text{(VIII)}$$

where L is the number of strata of X, N is the total number of units in the study area, Na is the number of units in stratum a, σ_a^2 is variance of Y in stratum a, and σ^2 is the variance Y across the entire study area.

The q-statistics measures the explanatory power of a variable X for the spatial distribution of Y. A q-value of 0 implies that X does not explain Y, while a q-value of 1 indicates that the spatial distribution of Y is completely determined by X. In addition, K-means clustering was employed to classify areas based on their energy balance characteristics, enabling the identification of patterns and intensities of UHI effects (Feng *et al.*, 2024). This clustering method grouped areas with similar LULCC traits, uncovering distinct zones with varying UHI intensities and characteristics. By categorizing these zones, the analysis of spatial patterns became more straightforward, allowing for a deeper understanding of localized impacts of land cover change and facilitating distinction between effects originating from the urban core and those from peripheral regions.

2.6. LULCC and UHI decadal variation analysis during extreme hot and dry events

In this study, we assessed how LULCC influences UHI intensity during extreme hot and dry conditions. A 30-year (1993 – 2023) analysis was conducted using the ERA5 temperature dataset. Extreme events were defined as periods during which the daily maximum temperature surpassed the 90th percentile of seasonal norms for at least three consecutive days (Equation IX), following established methodologies (Wu *et al.*, 2023; Zhang *et al.*, 2023). This threshold ensures the exclusion of transient heat spikes while capturing sustained thermal extremes. The study specifically examined how LULCC – such as urbanization-driven impervious surface expansion, deforestation, and the loss of green-blue infrastructure – modulates UHI intensity under extreme conditions. For instance, regions undergoing rapid conversion of vegetated land to built-up areas exhibited sharper increases in UHI intensity during heatwaves, primarily due to reduced evapotranspiration and increased heat storage. Trend analysis further linked decadal LULCC patterns to long-term UHI intensification, highlighting the role of surface albedo and aerodynamic resistance in exacerbating urban warming during climatic extremes.

$$T_{thresh} = percentile\ (T_{dmax}, 90) \quad \text{(IX)}$$

Where, T_{thresh} denotes the extreme temperature threshold, T_{dmax} is the daily maximum temperature, and *percentile* refers to the 90th percentile calculation of the dataset.

3. Results

3.1. Land change analysis of Zhengzhou city, Henan, China

The analysis of LULCC in Zhengzhou city, Henan, China, over the past three decades reveals profound transformations in the urban landscape, driven by rapid urbanization and socio-economic advancements. These forces have significantly reshaped the region. Covering a total area of 7,567 sqkm, Zhengzhou has experienced significant shifts in its land cover classes between 1993 and 2023, emphasizing the dynamic nature of its development. Over this period, built-up areas expanded considerably, reflecting the city's growth as a key economic and infrastructural hub. This expansion occurred alongside a reduction in agricultural lands and shrub-dominated areas, signaling the trade-offs inherent in urban growth. The surge in built-up areas, particularly after 2000, is closely associated with Zhengzhou's designation as a critical node in the Zhongyuan Urban Agglomeration, which fueled extensive construction and infrastructural investments. Concurrently, green spaces, including forests and farmlands, have been converted into residential, commercial, and industrial zones or fragmented due to urban encroachment.

Figure 3 vividly depicts the dynamic transformations in Zhengzhou city's land cover over the past three decades, revealing striking trends in urbanization and their environmental consequences. Built-up areas expanded substantially, increasing from 1,951.13 sqkm in 1993 to 4,502.84 sqkm in 2023 – an astounding growth of 130.78%. This rapid urban sprawl is emblematic of Zhengzhou's accelerated economic development and modernization, characterized by extensive infrastructure projects and industrial expansion. However, such growth is not without its challenges, as it often comes at the expense of natural landscapes and agricultural zones, leading to significant ecological and environmental degradation.

For instance, farmlands experienced a dramatic decline, shrinking from 3,822.71 sqkm in 1993 to 1,112.35 sqkm in 2023 – a staggering reduction of 70.90%. This loss raises critical concerns about the long-term sustainability of agricultural activities and the implications for local food security. The conversion of farmlands into urban spaces reflects the growing demand for land to accommodate an expanding population and burgeoning economic activities, stressing the tension between development and agricultural sustainability.

Similarly, forest areas diminished from 225.32 sqkm in 1993 to 127.60 sqkm in 2023, representing a reduction of 43.37%. This decline underscores the environmental pressures associated with urban expansion, as forests play a pivotal role in mitigating climate change through

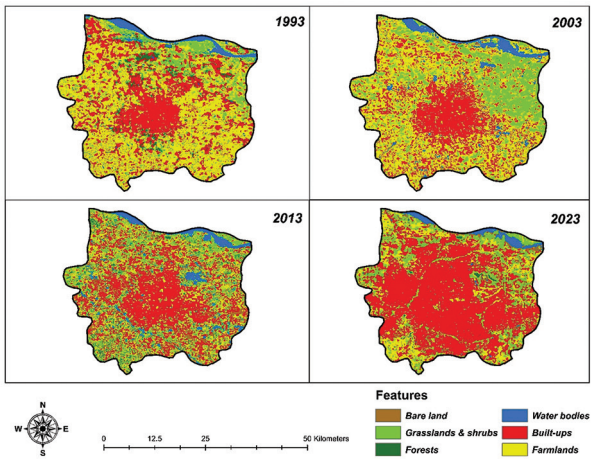

Figure 3. Land use and land cover change over the past three decades in Zhengzhou city, Henan, China
Source: Maps by the authors

carbon sequestration, regulating hydrological cycles, and supporting biodiversity. The reduction in forest cover not only compromises these ecological functions but also exacerbates the UHI effect, as vegetative cooling is replaced by heat-absorbing urban surfaces. Grasslands exhibited fluctuations over the study period, transitioning into other land cover types such as bare lands or built-up areas. This variability reflects the vulnerability of grasslands to urbanization pressures and land degradation. While some reforestation and greening initiatives may have offset these losses in specific locations, the overall trend reveals a marked decline in vegetative cover, contributing to rising LST and intensified UHI effects.

The data presented in Tables 2-4 offer a detailed examination of the temporal and spatial dynamics of LULCC in Zhengzhou city over the study period. These findings illuminate profound transformations in land cover classes and underscore their implications for urban sustainability, environmental health, and long-term ecological stability. Table 2 provides a snapshot of the total area covered by each land cover class over the specified years, capturing the shifts resulting from rapid urbanization. Built-up areas experienced a dramatic increase, expanding from 1,951.13 sqkm in 1993 to 4,502.84 sqkm in 2023, reflecting a 130.78% growth. This surge highlights the city's infrastructural expansion and population growth. However, this development came at the cost of significant reductions in farmlands and forests, which decreased by 70.90% and 43.37%, respectively. Farmlands shrank from 3,822.71 sqkm in 1993 to 1,112.35 sqkm in 2023, raising concerns about food security and the resilience of the agricultural sector. Similarly, forested areas declined from 225.32 sqkm to 127.60 sqkm, emphasizing the environmental toll of urban expansion.

An accuracy assessment for Zhengzhou city was conducted using user accuracy, producer accuracy, and the Kappa coefficient to validate the classification results. A total of 600 sample points (100 per land-use class) were generated for each study year (1993, 2003, 2013, and 2023) and validated using Google Earth Pro (version 7.3). The classification accuracy rates for 1993, 2003, 2013, and 2023 were 92.67%, 92.33%, 92.83%, and 92.17%, respectively, yielding an average accuracy rate of 92.50% over the study period (Appendix).

The temporal dynamics as presented in Table 3 reveal a consistent annual increase in built-up areas,

Table 2. Area coverage for each land cover class (sqkm), 1993 – 2023

Class	1993	2003	2013	2023
Built-up	1,951.13	2,101.20	2,409.59	4,502.84
Farmlands	3,822.71	3,256.13	2,229.66	1,112.35
Forests	225.32	205.85	192.87	127.60
Water bodies	334.71	389.51	424.18	370.91
Bare land	484.79	255.83	1,160.22	381.20
Grasslands & shrubs	748.34	1,358.49	1,150.48	1,072.09

Note: Total area coverage: 7,567 sqkm.

Table 3. Temporal variations in Zhengzhou city's land cover changes (%), 1993 – 2023

Class	1993 – 2003	2003 – 2013	2013 – 2023	1993 – 2023
Built-up	+7.69	+14.68	+86.87	+130.78
Farmlands and shrubs	−14.82	−31.52	−50.11	−70.90
Forests	−8.64	−6.31	−33.84	−43.37
Water bodies	+16.37	+8.90	−12.56	+10.82
Bare land	−47.23	353.51	−67.14	−21.37
Grasslands and shrubs	+81.53	−15.31	−6.81	+43.26

Table 4. Rate and magnitude of change (sqkm) in land cover classes of Zhengzhou city, 1993 – 2023

Class	1993	2023	Magnitude of change (sqkm)	Rate of change (year [%])	Magnitude of change (sqkm/year)
Built-up	1,951.13	4,502.84	+2,551.71	+4.36	+85.06
Farmlands and shrubs	3,822.71	1,112.35	−2,710.36	−2.36	−90.35
Forests	225.32	127.60	−97.72	−1.45	−3.26
Water bodies	334.71	370.91	+36.20	+0.36	+1.21
Bare land	484.79	381.20	−103.59	−0.71	−3.45
Grasslands and shrubs	748.34	1,072.09	+323.75	+1.44	+10.79

averaging 4.36% per year. This trend underscores the city's rapid urbanization, driven by economic growth and demographic pressures. Conversely, farmlands and forests exhibited negative annual growth rates of −3.24% and −1.33%, respectively, illustrating the trade-offs inherent in urban development. The gradual yet persistent decline in these natural and semi-natural landscapes highlights the vulnerability of ecological systems to urban sprawl. The sustained loss of farmlands is particularly alarming, as it not only threatens food production but also diminishes the natural cooling effects provided by vegetation, contributing to the intensification of the UHI effect. The reduction in forested areas further compounds this problem, given the vital role of forests in sequestering carbon, regulating temperature, and supporting ecological stability.

The analysis of change rates and magnitudes in Table 4 sheds further light on the intensity of LULCC in Zhengzhou city. Built-up areas recorded the highest rate and magnitude of change, emphasizing the aggressive pace of urbanization. Between 1993 and 2023, the city's expansion significantly outpaced the regeneration or preservation of natural landscapes. Farmlands exhibited the greatest absolute loss, accounting for a reduction of over 2,700 sqkm, while forests experienced a smaller but still substantial proportional decline.

3.2. LST and UHI analysis

The relationship between land cover changes and LST is critical to understanding the UHI effect, a phenomenon where urban areas experience elevated temperatures compared to their rural surroundings due to extensive land cover alterations and intensified human activities. Over the past three decades, Zhengzhou city has undergone rapid urbanization, profoundly altering its thermal environment.

Figure 4 provides a graphical representation of LST variations during this period, revealing a marked increase in average temperatures across the city. The data highlight that the average LST in urban zones rose from 25.72°C in 1993 to 31.49°C in 2023, representing a staggering 22.4% increase (+5.8°C). This warming trend is most pronounced during the summer, where the combination of reduced vegetation, increased impervious surfaces, and anthropogenic heat emissions amplifies thermal conditions. The findings strongly correlate the expansion of built-up areas with elevated LST values, emphasizing the role of land cover transitions in driving local climate change.

Figure 5 delves deeper into the trends of UHI intensity in Zhengzhou city, presenting a clear and consistent pattern of intensification over the last three decades. UHI intensity – measured as the temperature difference between urban and rural areas – increased from 1.02°C in 1993 to 2.49°C in 2023, representing a striking 144% increase (+1.5°C). This significant amplification is closely linked to the expansion of impervious surfaces, the loss of vegetative cover, and sprawling urban infrastructure. The summer months exhibit the highest UHI intensities, reflecting the compounded effects of solar radiation, reduced evapotranspiration, and the heat-retaining properties of urban materials such as asphalt and concrete.

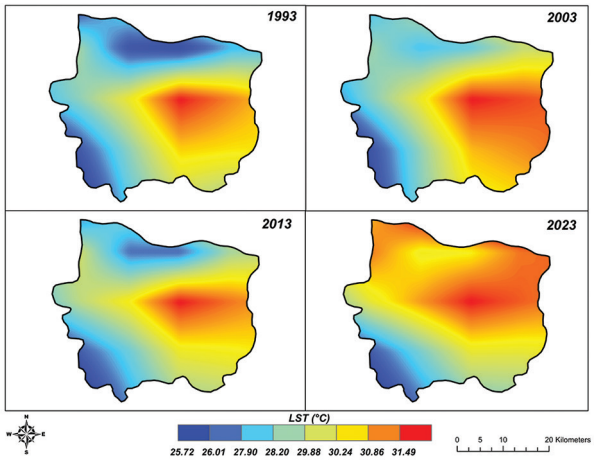

Figure 4. Land surface temperature (LST) variations in Zhengzhou city, Henan, China (1993 – 2023)
Source: Maps by the authors

3.3. Land metrics and UHI

The correlation between various land cover types and UHI intensity is pivotal for understanding the mechanisms driving urban temperature variations. The analysis of land metrics reveals the critical influence of different land cover types on the thermal dynamics of urban environments, providing essential insights for urban planning and sustainable development strategies.

Figure 6 presents the results of a correlation analysis, offering a clear depiction of the relationships between land cover types and UHI intensity. Built-up areas demonstrate a strong positive correlation with UHI intensity (r = 0.729), signifying that the expansion of impervious surfaces substantially contributes to increased heat retention within urban settings. This correlation is driven by the thermal properties of urban materials, such as asphalt and concrete, which have high heat storage capacities and low albedo, thereby absorbing and re-radiating more solar energy. The urbanization process, characterized by the replacement of natural landscapes with impervious surfaces, disrupts the natural energy balance by reducing evapotranspiration and increasing sensible heat flux. As built-up areas expand, these effects

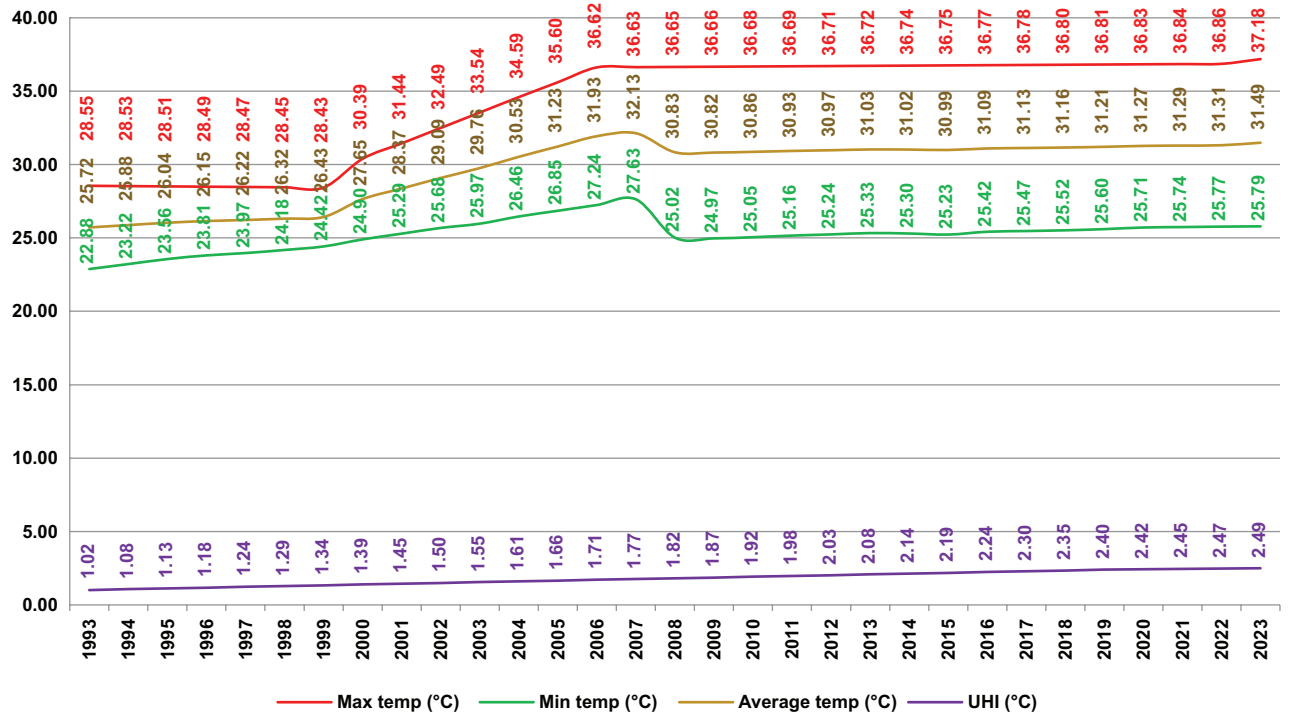

Figure 5. Zhengzhou city's land surface temperature and urban heat island trends over the past 30 years
Source: Graph by the authors

intensify, contributing to the observed rise in LST and exacerbating UHI intensity.

Conversely, vegetated areas, including farmlands, forests, water bodies, and grasslands and shrubs, exhibit negative correlations with UHI intensity, stressing their mitigating effects on urban temperatures. Forests display the strongest negative correlation (r = −0.962), followed by farmlands (r = −0.891), reflecting their role in cooling urban microclimates through processes such as evapotranspiration and shading. Forests enhance latent heat flux and reduce the amount of solar energy absorbed by the ground, thereby moderating local temperatures. Grasslands, while slightly less effective than forests, also show a significant negative correlation with UHI intensity (r = −0.739). Grasslands contribute to cooling by maintaining lower surface temperatures and facilitating air circulation, which helps dissipate heat.

The statistical analysis (Table 5) of LST and UHI in Zhengzhou city from 1993 to 2023 further reveals significant trends and relationships. Mean LST increased steadily from 25.72°C in 1993 to 31.49°C in 2023, reflecting a warming trend driven by rapid urbanization and land cover changes. UHI intensity also showed a marked increase, rising from 1.02°C in 1993 to 2.49°C in 2023, indicating a growing thermal disparity between urban and rural areas. The p-values for all years were <0.001, confirming the statistical significance of these trends. The correlation between land cover changes and UHI intensity, as measured by R^2 values, strengthened over time – from 0.729 in 1993 to 0.792 in 2023 – highlighting the growing influence of urbanization on local thermal dynamics. In addition, the high Kappa coefficients (ranging from 0.89 to 0.92) demonstrate the robustness and accuracy of the land cover classification, further supporting the reliability of the findings. These results underscore the profound impact of urbanization on Zhengzhou's thermal environment and emphasize the need for sustainable urban planning to mitigate UHI effects.

3.4. Geodetector and clustering analysis

The Geodetector analysis was employed to quantitatively assess the impact of LULCC on the UHI effect in Zhengzhou city. This spatial statistical approach provides robust insights into the extent to which different land cover types contribute to variations in LST, unveiling the complex interplay between urbanization and thermal dynamics. As shown in Figure 6, the q-statistics derived for key land cover types – built-up, bare land, farmland, grasslands and shrubs, forest, and water bodies – reveal distinct patterns of influence. The analysis identifies built-up areas as the most influential factor, with the highest

q-statistic value ranging between 0.75 and 0.85 over the past three decades. This indicates a strong and statistically significant relationship between urbanization and elevated UHI. The predominance of impervious surfaces, such as concrete, asphalt, and rooftops, combined with reduced evapotranspiration and altered albedo, significantly contributes to the absorption and retention of heat.

Forests and grasslands and shrubs exhibit q-statistic values between 0.35 and 0.55, respectively, indicating moderate to weak associations with UHI intensity variations. Although these land cover types have lower thermal inertia compared to urban areas, the lack of vegetation in bare land and the seasonal variability in forests can influence localized temperature dynamics. Farmland demonstrates q-statistic values ranging from 0.55 to 0.75, indicating a significant cooling effect on urban thermal environments. Vegetation-dominated landscapes mitigate UHI through evapotranspiration, shading, and reduced heat storage, emphasizing their critical role in countering the adverse impacts of urbanization. However, the slightly lower q-statistic value for forests compared to grasslands and shrubs may reflect spatial fragmentation, degradation, or changes in forest density over time.

Table 5. Statistical results of land surface temperature (LST) and urban heat island intensity (UHI) analysis for Zhengzhou city, Henan, China, 1993 – 2023

Year	Mean LST (°C)	UHI (°C)	p-value	R^2	Kappa coefficient
1993	25.72	1.02	<0.001	0.729	0.89
2003	27.45	1.35	<0.001	0.745	0.91
2013	29.12	1.98	<0.001	0.768	0.90
2023	31.49	2.49	<0.001	0.792	0.92

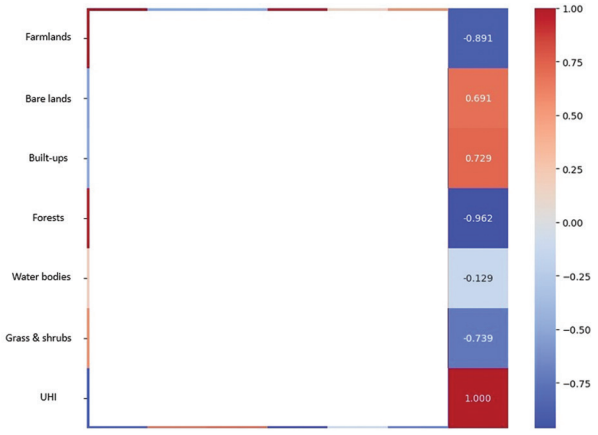

Figure 6. Correlation analysis between land cover types and urban heat island intensity
Source: Heatmap by the authors

The K-means clustering analysis provides deeper insights into the spatial patterns and impacts of LULCC on UHI intensity in Zhengzhou city. As shown in Figures 7 and 8, the clustering results classified the city into six distinct clusters based on the interaction between various land cover types and their influence on UHI. This spatial categorization highlights the complex relationship between urbanization, vegetation, and thermal dynamics. Clusters 1 and 2, predominantly characterized by high proportions of farmlands, water bodies, forests, and grasslands and shrubs, exhibited the lowest UHI intensities. These clusters represent areas dominated by natural surfaces, where evapotranspiration and evaporative cooling significantly reduce surrounding land temperatures. The presence of cooling features, such as forests, farmlands, grasslands, shrubs, lakes, reservoirs, and ponds, plays a crucial role in mitigating UHI effects.

In contrast, Clusters 5 and 6, characterized by extensive built environments, exhibit significantly elevated UHI effects. This is primarily attributed to the dominance of impervious surfaces, such as concrete and asphalt, which absorb and retain heat during the day and release it slowly at night. This contributes to higher local temperatures compared to surrounding rural areas. The sparse presence of vegetation and the prevalence of bare lands further exacerbate this phenomenon, as bare soils absorb heat without offering the cooling benefits associated with vegetation. In addition, the dense configuration of buildings and infrastructure, combined with bare lands, reduces opportunities for cooling through evapotranspiration and increases heat retention. Human activities, including transportation and energy consumption, further amplify heat generation in these urbanized settings.

The combined findings from the Geodetector and K-means clustering analyses, visualized in Figure 8, provide significant insights into the temporal dynamics of LULCC and their implications for UHI intensity over the past 30 years. These results underscore the profound impact of urbanization on thermal dynamics within Zhengzhou city, offering a comprehensive understanding of the mechanisms driving UHI variations. The temporal analysis also reveals a striking 130.78% increase in built-up areas from 1993 to 2023, driven by rapid urbanization and industrial expansion. This urban growth has directly correlated with a substantial rise in LST, with average LSTs increasing by approximately 5.77°C over the three decades. Such temperature escalations highlight the intensification of the UHI phenomenon, driven by the proliferation of impervious surfaces, which absorb and retain heat more efficiently than natural landscapes.

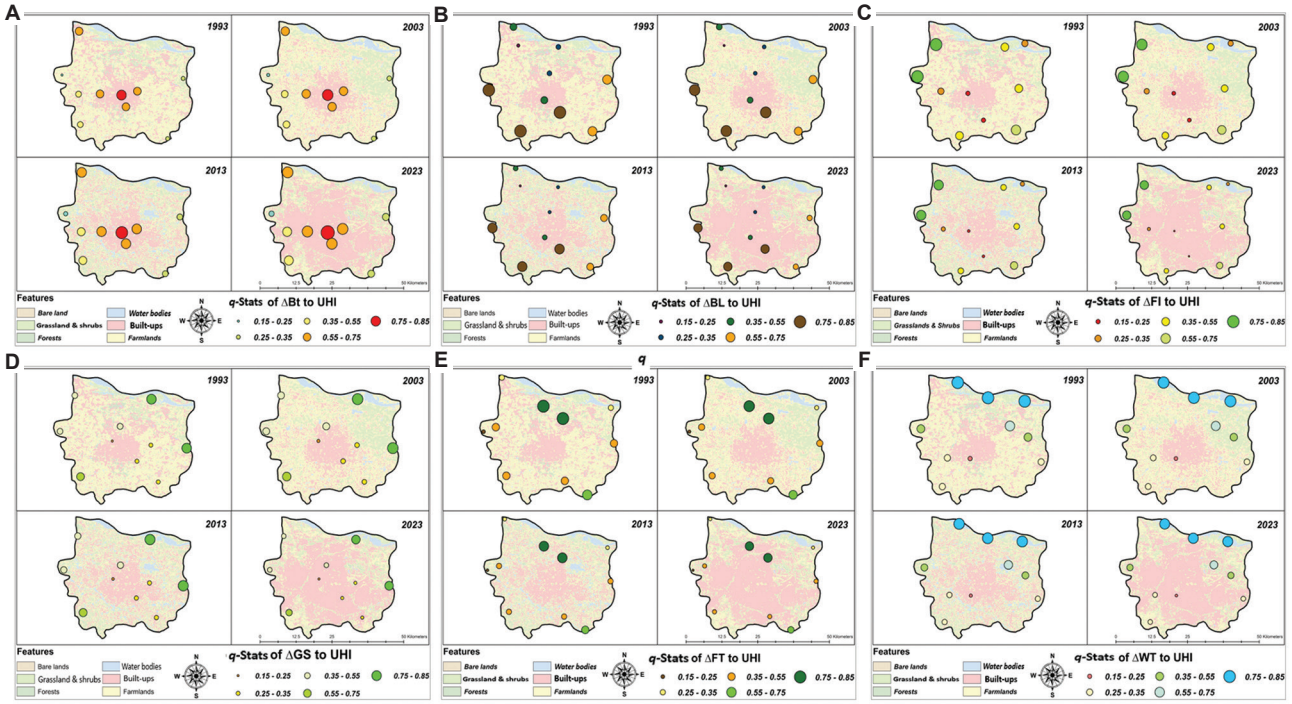

Figure 7. *q*-statistics (q-stats) output showing the effects of changes (Δ) in (A) built-up (Bt), (B) bare land (BL), (C) farmland (Fl), (D) grasslands & shrubs (GS), (E) forest (FT), and (F) water bodies (WT) to urban heat island (UHI) variability in Zhengzhou city, Henan, China
Source: Maps by the authors

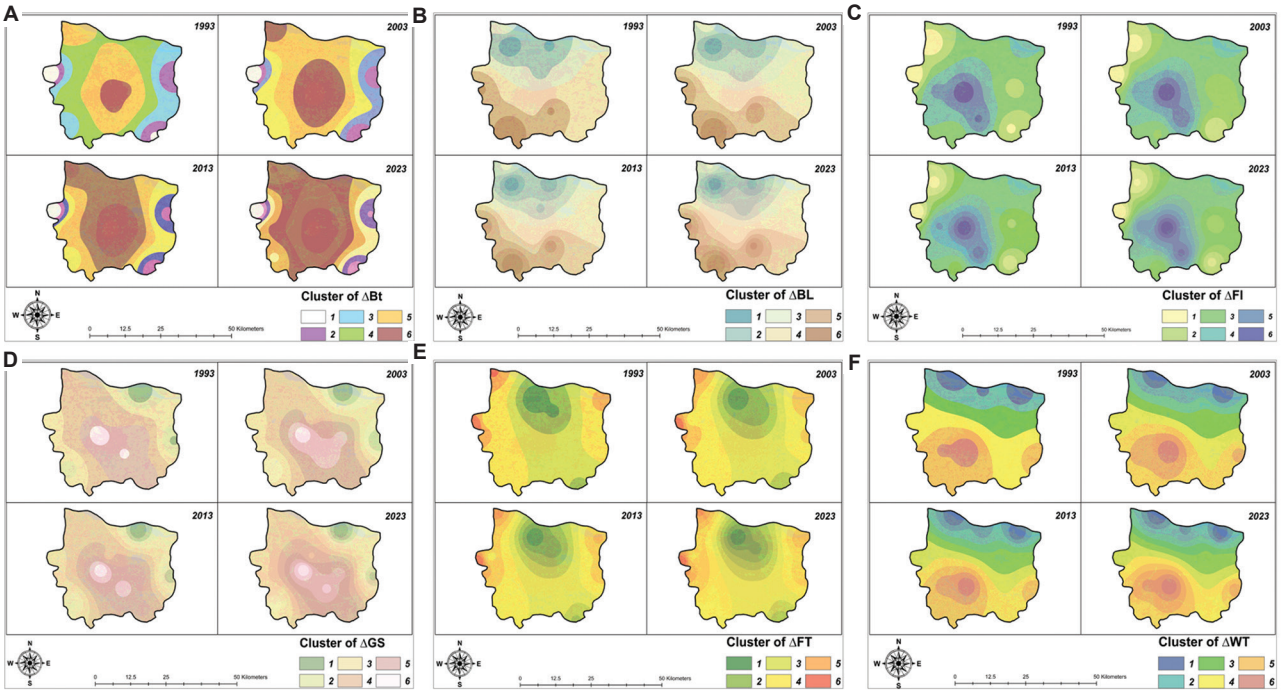

Figure 8. K-means output of cluster effect of changes (Δ) in (A) built-up (Bt), (B) bare land (BL), (C) farmland (Fl), (D) grasslands & shrubs (GS), (E) forest (FT), and (F) water bodies (WT) to urban heat island (UHI) variations in Zhengzhou city, Henan, China
Source: Diagrams by the authors

3.5. LULCC influence on UHI decadal variation during extreme hot and dry events

Based on the decadal LULCC and UHI interaction during extreme dry and hot events (Figures 9-10 and Figure A1), the multi-temporal analysis reveals a pronounced transformation in LULCC composition and its associated impacts on LST (Figure A1) and UHI intensity (Figures 9-10) across three distinct decades: 1993 – 2003, 2003 – 2013, and 2013 – 2023. This temporal breakdown highlights a clear trajectory of urban expansion at the expense of vegetative cover, underscoring the critical role of anthropogenic alterations in exacerbating thermal stress during heat extremes. During the initial decade, built-up areas constituted a relatively modest proportion of the LULC, averaging 13 – 15% across the peak summer months (June to August). Forests and farmlands were the dominant land covers, each maintaining coverage above 18%, while grasslands and shrubs also contributed significantly to the landscape matrix. Correspondingly, LST values remained relatively moderate, peaking at approximately 31.5°C in July and dipping to around 29.5°C in June (Figure A1). The average UHI intensity for this period was 1.7°C, indicating relatively limited urban-induced thermal amplification (Figures 9-10). This finding suggests that the relatively high presence of vegetative covers, particularly forests and farmlands, played a crucial role in mitigating surface heating, likely through enhanced evapotranspiration and shading effects.

The second decade marks a notable shift toward urban land expansion. Built-up areas increased sharply, reaching over 22% by June and rising to about 24% in August. This expansion came at the expense of both forests and farmlands, which saw appreciable declines in coverage. Forests dropped below 16%, and grasslands also exhibited contraction, reflecting a broader pattern of ecological degradation. This land transformation coincided with an uptick in LST values, which now ranged from approximately 30.5°C in June to 33.5°C in July (Figure A1). More critically, the average UHI value rose to 2.4°C (Figures 9-10), highlighting a more intensified urban heat effect during extreme hot events. These findings underscore the thermal penalties associated with increased impervious surfaces and diminished vegetative buffers, where reduced albedo and altered surface energy balances collectively amplify heat accumulation. The most recent decade (2013 – 2023) reveals an alarming surge in built-up area coverage, exceeding 30% across all summer months, with a peak of over 32% in July. Concomitantly, forest, farmland, and grassland covers have declined to below 13%, with some categories approaching only 10% coverage. This

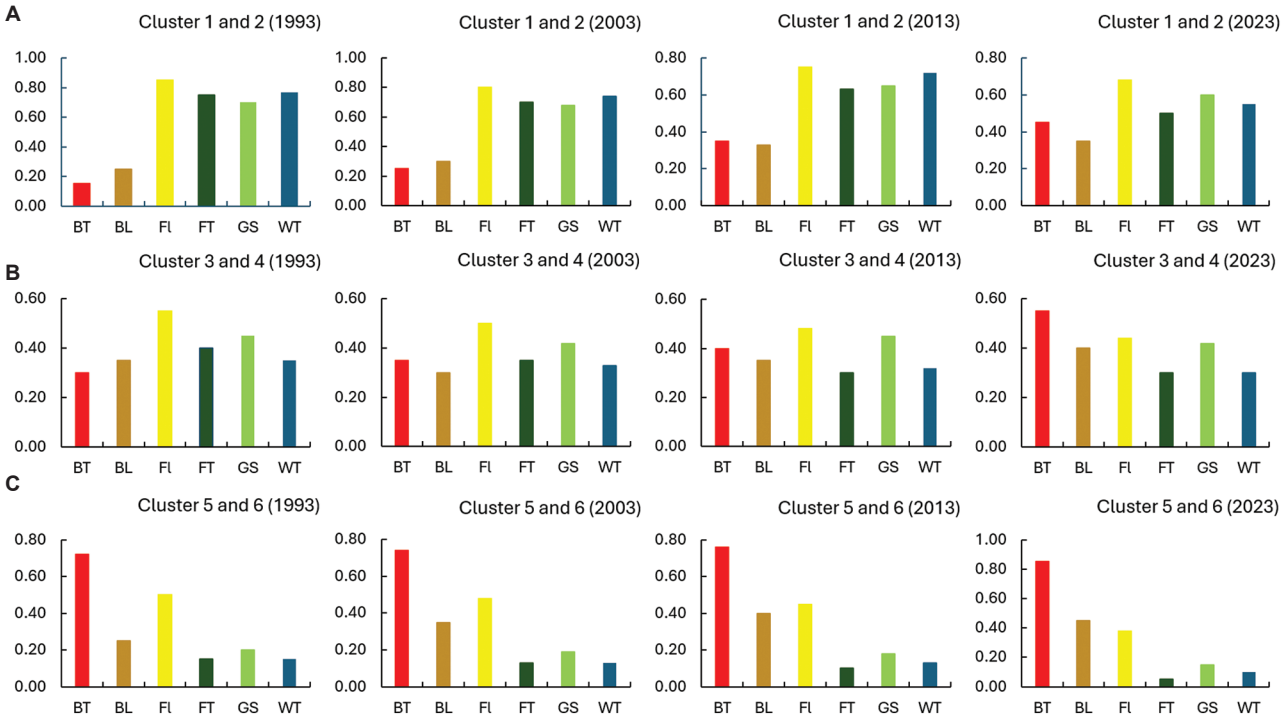

Figure 9. *q*-statistics and K-means cluster graph outputs of the land use and land cover change over the past 30 years. (A) Clusters 1 and 2. (B) Clusters 3 and 4. (C) Clusters 5 and 6
Abbreviations: Bt: Built-up; BL: Bare land; Fl: Farmland; GS: Grasslands and shrubs; FT: Forest; WT: Water bodies
Source: Graphs by the authors

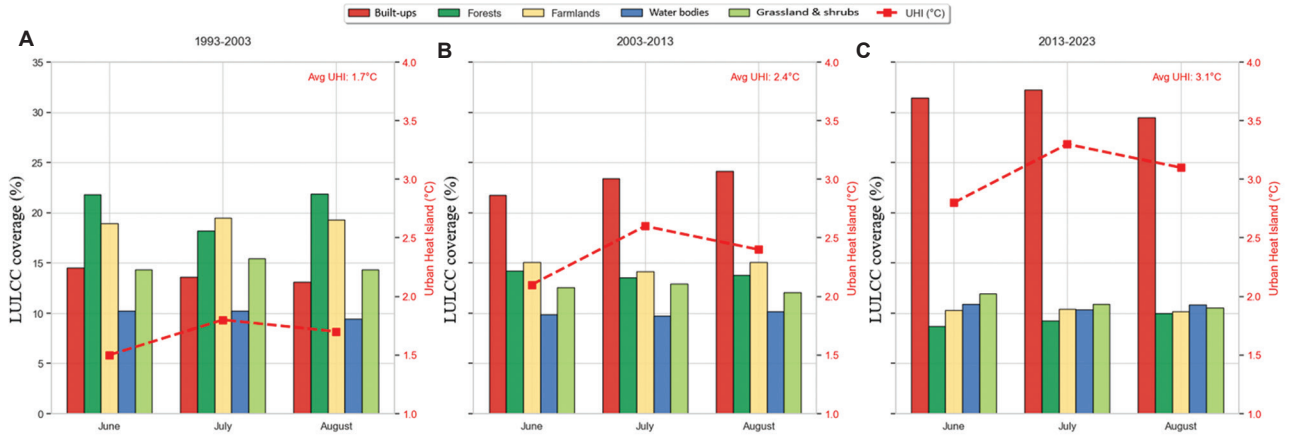

Figure 10. The effects of land use and land cover change on urban heat island during extreme hot and dry events in Zhengzhou city, Henan, China, over the past 30 years (1993 – 2023). (A) 1993 – 2003; (B) 2003 – 2013; (C) 2013 – 2023
Source: Graphs by the authors

severe vegetative loss has had profound implications for thermal dynamics. LST values soared, peaking near 36.5°C in July and remaining elevated in the adjacent months (Figure A1). The corresponding UHI intensity reached an average of 3.1°C (Figures 9-10), marking the highest value recorded across all decades. This clearly demonstrates the cumulative effect of sustained urban encroachment and vegetative decline, which not only raises mean surface temperatures but also exacerbates the risk and severity of UHIs during climatologically extreme periods.

4. Discussion

4.1. Land use change, LST, and UHI dynamics

The findings from this study corroborate existing literature, highlighting the profound impact of LULCC on UHI effects. Zhengzhou's rapid urbanization over the past three decades has resulted in a substantial increase in built-up areas, correlating strongly with elevated LST. The average LST in urban zones rose from 25.72°C in 1993 to 31.49°C in 2023, reflecting an increase over this period. This aligns with observations from other rapidly urbanizing regions, such as those documented by Oke (1982) and Huang *et al.* (2013), who reported similar UHI intensifications in Beijing and Guangzhou, respectively. These studies highlight the role of urban expansion and its associated thermal impacts, driven by the widespread use of construction materials with high heat storage capacities and low albedo, as noted by Mohajerani *et al.* (2017) and Taha *et al.* (1988). The significant positive correlation between built-up areas and UHI intensity (r = 0.729) further emphasizes the critical role of impervious surfaces in shaping urban thermal dynamics. This finding resonates with prior studies, such as Liu *et al.* (2024), which demonstrated that urbanization-driven replacement of natural vegetation with heat-absorbing materials exacerbates surface warming. The data also revealed that UHI intensity in Zhengzhou increased from 1.02°C in 1993 to 2.49°C in 2023, reflecting a staggering rise. Such intensifications not only signify the thermal burden of urban growth but also highlight the urgent need to adopt mitigation strategies that balance development with environmental sustainability.

In addition, the loss of vegetative cover – approximately 70.90% of farmlands and 43.37% of forest areas – has contributed to diminished cooling effects, further amplifying UHI phenomena. Vegetation plays a crucial role in mitigating urban warming through mechanisms such as evapotranspiration, shading, and increased surface albedo. Research by Bowler *et al.* (2010) and Yang *et al.* (2017) corroborates this finding, showing that green spaces can reduce LST by up to 2°C in urban environments. The decline in natural buffers within Zhengzhou highlights the pressing need to preserve and expand vegetative cover to counteract rising urban temperatures.

Comparative analyses of UHI intensity across different land cover types in this study revealed that areas with high proportions of built-up land consistently exhibit higher LST values, whereas vegetated areas, including farmlands, forests, grasslands and shrubs, and water bodies, contribute significantly to temperature reduction. For instance, neighborhoods with integrated green infrastructure were found to exhibit up to 2°C lower temperatures compared to densely urbanized zones. These findings are aligned with research by Gunawardena *et al.* (2017), which highlights the effectiveness of urban greenery in mitigating UHI effects. Furthermore, the temporal and spatial heterogeneity of UHI effects in Zhengzhou aligns with studies conducted

in other global urban centers, such as New York, United States (Voogt & Oke, 2003), and Tokyo, Japan (Fujibe, 2009). These studies similarly reported that areas with mixed land use – combining urban and vegetative cover – exhibit lower UHI intensities compared to homogeneous built-up zones. Their findings reinforce the importance of urban design strategies that integrate green spaces, water bodies, and permeable surfaces to mitigate UHI effects.

The findings of the present study emphasize the need for proactive urban planning that prioritizes sustainable practices to combat UHI effects. Strategies such as implementing green roofs, increasing tree canopy cover, and preserving natural landscapes can significantly alleviate urban thermal stress. As Zhengzhou continues to urbanize, these results serve as a crucial call to action for policymakers to adopt evidence-based solutions to promote thermal resilience, enhance environmental quality, and ensure the long-term sustainability of urban ecosystems.

4.2. The cooling effects of vegetation and water bodies on urban thermal dynamics

The observed negative correlation between vegetated areas, such as farms, forests, and grasslands and shrubs, and UHI intensity highlights the essential role of vegetation in regulating urban temperatures. The strong negative correlation for forests ($r = -0.962$) aligns with studies such as Bowler *et al.* (2010), which demonstrate that urban green spaces mitigate ambient temperatures through mechanisms such as evapotranspiration, shading, and increased albedo. Similarly, Zhang *et al.* (2020) emphasized that vegetation enhances latent heat flux, reducing surface temperatures and cooling the surrounding microclimate. The analysis reveals a significant reduction in forest cover in Zhengzhou, decreasing from 225.32 sqkm in 1993 to 127.60 sqkm in 2023—a loss of nearly 43%. This decline has directly intensified UHI effects, as vegetation loss diminishes the natural cooling functions provided by green spaces. This finding mirrors trends in other urban centers, such as New York city, United States, where Lafortezza *et al.* (2009) documented that the reduction of green spaces exacerbated heat stress during extreme weather events, particularly heatwaves. The substantial loss of vegetative cover in Zhengzhou underscores the critical need for urban greening initiatives to counteract rising UHI intensity. Strategies such as large-scale tree planting, reforestation, and the integration of green roofs and vertical gardens can play pivotal roles in restoring the cooling benefits of vegetation. These approaches not only lower surface and ambient temperatures but also enhance air quality, improve urban biodiversity, and provide aesthetic and recreational benefits for residents. Moreover, targeted urban planning that integrates vegetative buffers into built-up areas could mitigate UHI intensity while promoting climate resilience. For example, increasing forested areas around densely urbanized zones or embedding green corridors within the urban fabric can create microclimatic cooling zones that alleviate the thermal burden on the city. As urban expansion continues, these nature-based solutions represent a sustainable path forward, balancing development needs with environmental stewardship to foster healthier and more livable urban environments.

The findings from this study also highlight the significant role of water bodies in mitigating LST and reducing UHI intensity, as evidenced by their q-statistic value between 0.35 and 0.55. This result aligns closely with the work of Peng *et al.* (2020), who emphasized the cooling effects of urban water features on their surrounding environments. The notably low average LST observed in areas dominated by water bodies (27°C) stresses their effectiveness in moderating urban temperatures, even in regions experiencing significant urbanization. The integration of blue infrastructure into urban planning emerges as a crucial strategy for UHI mitigation. Water bodies, such as lakes, rivers, ponds, and reservoirs, contribute to localized cooling through processes such as evaporation, increased latent heat flux, and their natural high thermal inertia, which buffers temperature fluctuations. The preservation and enhancement of these aquatic features should therefore be prioritized as urban areas expand. This recommendation is further supported by findings from Li *et al.* (2024), who demonstrated that urban water bodies not only lower LST but also improve the thermal comfort of urban residents by reducing heat stress during extreme weather events. In addition, blue infrastructure offers multiple co-benefits, including improved biodiversity, recreational opportunities, enhanced air quality, and stormwater management. For Zhengzhou city, integrating water bodies into urban landscapes can serve as a sustainable approach to counteract UHI effects while fostering resilience to climate change. Urban design initiatives such as the creation of artificial wetlands, the restoration of natural waterways, and the incorporation of urban fountains and reflective water surfaces can amplify these benefits. Ultimately, a balanced integration of blue and green infrastructure within urban planning frameworks is essential for creating livable, thermally comfortable, and environmentally sustainable cities.

4.3. Spatial variability and UHI intensity

The K-means clustering analysis identified five distinct clusters of UHI intensity, underscoring the spatial heterogeneity of UHI effects across Zhengzhou. These findings align with conclusions drawn by Gago *et al.*

(2013), who highlighted that UHI intensity varies significantly within urban areas depending on local land cover characteristics. The clustering results pinpoint high-temperature zones predominantly composed of built-up areas, which are highly susceptible to severe heat stress. This emphasizes the critical need for targeted interventions, such as urban greening and reflective building materials, to mitigate the adverse thermal impacts in these densely urbanized regions. Additionally, the analysis revealed that areas with mixed land cover types exhibit lower LST values compared to clusters dominated by impervious surfaces. This observation corroborates the research by Zhao and Miao (2022), which demonstrated that the integration of green and blue spaces within urban areas can significantly reduce LST and alleviate UHI effects. Mixed land use not only enhances cooling through mechanisms such as evapotranspiration and shading but also improves air circulation, further contributing to thermal comfort.

These findings stress the importance of promoting land-use diversity as a key strategy for UHI mitigation. Urban planning initiatives that prioritize the integration of vegetation, water features, and permeable surfaces within built environments can effectively counteract the intensifying UHI effects driven by rapid urbanization. Moreover, the spatial variability highlighted by the clustering analysis offers valuable insights for policymakers, enabling them to design localized, context-specific interventions to enhance urban thermal resilience.

4.4. Policy recommendations

The results of this study highlight the profound implications of LULCC on urban thermal dynamics, particularly the exacerbation of UHI intensity across the observed decades in Zhengzhou city, Henan, China. The clear spatial and temporal correlations between expanding built-up areas, declining vegetation cover, and rising LST suggest an urgent need for a reorientation of urban development policies. This section outlines three key policy domains where actionable interventions could generate substantial environmental and public health co-benefits.

4.4.1. Urban greening and vegetation preservation

One of the most salient findings from the multi-decadal analysis is the persistent and spatially concentrated loss of vegetation, particularly in urban peripheries transitioning into high-density residential and commercial zones. This loss is directly linked to rising LST values and intensified UHI footprints, especially during summer. To address this, there must be a deliberate integration of green infrastructure into the urban fabric. Urban greening policies should go beyond ornamental landscaping to enforce strategic reforestation and conservation of existing tree cover, particularly in ecologically sensitive or high-risk thermal zones. Moreover, provincial authorities should introduce statutory minimum green cover requirements at the neighborhood level, embedded within local planning schemes. Public–private partnerships can be leveraged to co-finance community parks, green corridors, and vertical gardens on underutilized spaces such as rooftops and walls. The ecological services provided by urban vegetation – ranging from evapotranspiration and shading to carbon sequestration – make green infrastructure a non-negotiable component of heat mitigation strategies. In addition, preserving urban wetlands and riverine vegetation belts can contribute significantly to localized cooling effects and biodiversity conservation, underscoring the multifunctional value of green spaces.

4.4.2. Climate-sensitive urban planning and design

The analysis of UHI dynamics over the decades reveals a planning paradigm that has been largely reactive rather than anticipatory. In many of the thermally stressed zones identified in this study, high-density construction has proceeded with minimal consideration for thermal comfort, airflow patterns, or surface albedo. A paradigm shift toward climate-sensitive urban design is therefore imperative. This involves embedding heat risk assessments within planning approval processes and mandating passive cooling strategies as standard design features. Urban design guidelines should promote the use of high-albedo materials for pavements and rooftops, reduce street canyon effects through optimal building orientation, and preserve natural wind corridors to facilitate urban ventilation. Local governments can also explore the zoning of "cooling buffers"—green belts and open spaces between high-density developments. Importantly, climate-adaptive design must also be equitable; vulnerable communities in informal settlements should not be excluded from these interventions. Participatory planning approaches can be employed to ensure that climate-sensitive designs reflect local needs and knowledge while improving long-term thermal resilience.

4.4.3. Real-time urban climate monitoring and early warning systems

The temporal variability of LST and UHI intensity across the study period also underscores the importance of developing real-time climate monitoring systems that can inform dynamic and responsive governance. Currently, many cities lack the spatial granular and temporal frequency data necessary to understand microclimatic shifts, particularly those exacerbated by rapid land use transitions. Investing in urban sensor networks, complemented by satellite-derived LST data, can fill this

gap. These monitoring platforms should be institutionalized within urban governance structures, with data openly shared among planning agencies, emergency services, and the public. Early warning systems based on real-time thermal readings can trigger targeted interventions during extreme heat events, such as opening cooling centers or issuing heat advisories. Furthermore, long-term climate records from these systems can support iterative policy learning, allowing cities to evaluate the effectiveness of interventions and adapt them as urban conditions evolve.

4.5. Study limitations

This study has several limitations that warrant consideration. First, the reliance on remote sensing data for LULCC and LST analysis, while comprehensive, may not fully capture micro-scale variations in urban thermal dynamics. Ground-based measurements and finer spatial resolutions could provide a more detailed understanding of local temperature variations. Second, the study focuses on Zhengzhou, Henan, China, which limits the generalizability of the findings to cities with different climatic conditions, urban morphologies, or development trajectories. Third, while the temporal scope spans three decades, it may not fully account for potential nonlinearities in UHI evolution or the impacts of rapidly advancing technological developments, such as smart urban cooling systems. Finally, the smooth appearance of the LST maps in Figure 4 is due to the 30-m spatial resolution of Landsat imagery and interpolation techniques used during data processing. While this resolution captures broad temperature patterns, such as urban–rural contrasts, it may not fully resolve fine-scale heterogeneity caused by variations in building density, vegetation, or surface materials. Future studies could explore higher-resolution thermal data to better characterize microclimatic variations in urban environments.

5. Conclusion

In this study, we examined the influence of LULCC on UHI intensity under extreme hot and arid conditions. This study provides compelling evidence of the profound impact of LULCC on the intensification of UHI effects in Zhengzhou, Henan, China. Our findings reveal that rapid urbanization, marked by a 130.78% increase in built-up areas, has significantly contributed to a 144% rise in UHI intensity over three decades. Conversely, the loss of vegetative cover, particularly forests and farmlands, has exacerbated urban thermal conditions, reducing the natural cooling benefits provided by these landscapes. The Geodetector and K-means clustering analyses highlight the dominant role of built-up areas in driving UHI effects, while also underscoring the mitigating influence of green and blue spaces. These results emphasize the urgent need for sustainable urban planning strategies that prioritize the preservation and integration of vegetation and water bodies within urban landscapes. Such strategies can serve as critical tools for mitigating UHI effects, enhancing urban thermal comfort, and fostering climate resilience in rapidly growing cities. This study reinforces the importance of evidence-based policy interventions aimed at balancing urban expansion with environmental conservation. These efforts will be pivotal in guiding sustainable development and ensuring the well-being of urban populations amid the challenges posed by urbanization and climate change.

5.1. Policy implications and future research directions

The results of this study carry significant implications for urban policy and planning in Zhengzhou and other rapidly urbanizing cities. The findings emphasize the necessity for evidence-based policies that prioritize the integration of green and blue infrastructure into urban development plans. As urbanization continues to accelerate, it is crucial for policymakers to adopt sustainable land-use practices that enhance the resilience of urban environments to climate change. Measures such as increasing vegetative cover, restoring degraded ecosystems, and incorporating water bodies into urban layouts can significantly mitigate UHI effects while promoting ecological sustainability.

Future research should explore the long-term effectiveness of specific interventions aimed at mitigating UHI effects. Studies focusing on the implementation of green roofs, urban forestry, and the restoration of water bodies could provide valuable insights into best practices for urban heat management. In addition, while this study examined proportional land cover effects on UHI, landscape pattern metrics – such as patch shape and connectivity – may provide additional explanatory power and warrant future investigation. Furthermore, incorporating socio-economic factors, such as population density and energy use patterns, could provide a more holistic understanding of UHI dynamics. Modeling future UHI scenarios in response to projected urban growth and climate change, using advanced machine learning and simulation techniques, may offer critical guidance for sustainable urban planning. Cross-city comparative studies could also enrich our understanding of how different urban configurations influence UHI intensity and mitigation strategies.

Acknowledgment

We would like to express our gratitude to the Ministry of Education (MoE), the Henan Provincial Government, and Henan University for their support and resources that made this project possible.

Funding

This project was supported or funded by the 2024 Henan Provincial Postdoctoral Research Project (Grant No. HN2025115) (J25001Y).

Conflict of interest

Emmanuel Yeboah, Isaac Sarfo, and Clement Kwang are the Guest Editor of this special issue, but were not in any way involved in the editorial and peer-review process conducted for this paper, directly or indirectly. Separately, other authors declared that they have no known competing financial interests or personal relationships that could have influenced the work reported in this paper.

Author contributions

Conceptualization: Emmanuel Yeboah
Data curation: Emmanuel Yeboah
Formal analysis: Emmanuel Yeboah, Isaac Sarfo, Clement Kwang, Philip Kofi Alimo, Michael Atuahene Djan, Millicent Selase Afenya, Abraham Okrah
Investigation: Emmanuel Yeboah, Isaac Sarfo, Clement Kwang, Philip Kofi Alimo
Methodology: Emmanuel Yeboah, Isaac Sarfo, Clement Kwang
Resources: Solomon Obiri Yeboah Amankwah
Supervision: Solomon Obiri Yeboah Amankwah
Validation: Emmanuel Yeboah, Isaac Sarfo, Clement Kwang, Philip Kofi Alimo, Michael Atuahene Djan, Millicent Selase Afenya, Abraham Okrah
Visualization: Emmanuel Yeboah
Writing-original draft: Emmanuel Yeboah
Writing-review & editing: Isaac Sarfo, Clement Kwang, Philip Kofi Alimo, Michael Atuahene Djan, Millicent Selase Afenya, Abraham Okrah, Solomon Obiri Yeboah Amankwah

Ethics approval and consent to participate

Not applicable.

Consent for publication

Not applicable.

Availability of data

The data that back up the study's conclusions is accessible via the appropriate link provided in the Data and Methods section.

References

Bowler, D. E., Buyung-Ali, L., Knight, T. M., & Pullin, A. S. (2010). Urban greening to cool towns and cities: A systematic review of the empirical evidence. *Landscape and Urban Planning*, *97*(3):147-155.

Cai, E., Bi, Q., Lu, J., & Hou, H. (2022). The spatiotemporal characteristics and rationality of emerging megacity urban expansion: A case study of Zhengzhou in central China. *Frontiers in Environmental Science*, *10*:860814.

https://doi.org/10.3389/FENVS.2022.860814/BIBTEX

Chen, X., Wang, Z., Yang, H., Ford, A. C., & Dawson, R. J. (2023). Impacts of urban densification and vertical growth on urban heat environment: A case study in the 4th Ring Road Area, Zhengzhou, China. *Journal of Cleaner Production*, *410*:137247.

https://doi.org/10.1016/J.JCLEPRO.2023.137247

Feng, J., Zhang, K., Xu, Z., Du, C., Tang, X., & Zhang, L. (2024). Quantitative study on color characteristics of urban park landscapes based on K-means clustering and SD. method. *Earth Science Informatics*, *17*(2):999-1012.

Fujibe, F. (2009). Detection of urban warming in recent temperature trends in Japan. *International Journal of Climatology*, *29*(12):1811.

Gago, E. J., Roldan, J., Pacheco-Torres, R., & Ordóñez, J. (2013). The city and urban heat islands: A review of strategies to mitigate adverse effects. *Renewable and Sustainable Energy Reviews*, 25:749-758.

Grover, A., & Singh, R. B. (2015). Analysis of urban heat island (UHI) in relation to normalized difference vegetation index (NDVI): A comparative study of Delhi and Mumbai. *Environments*, *2*:125-138.

https://doi.org/10.3390/ENVIRONMENTS2020125

Gunawardena, K. R., Wells, M. J., & Kershaw, T. (2017). Utilising green and bluespace to mitigate urban heat island intensity. *Science of the Total Environment*, *584*:1040-1055.

Han, J., Mo, N., Cai, J., Ouyang, L., & Liu, Z. (2024). Advancing the local climate zones framework: A critical review of methodological progress, persisting challenges, and future research prospects. *Humanities and Social Sciences Communications, 11*(1):1-18.

https://doi.org/10.1057/s41599-024-03072-8

Hu, Y., Connor, D. S., Stuhlmacher, M., Peng, J., & Turner, B. L. (2024). More urbanization, more polarization: Evidence from two decades of urban expansion in China. *NPJ Urban Sustainability*, *4*(1):1-11.

https://doi.org/10.1038/s42949-024-00170-z

Huang, B., Wang, J., Song, H., Fu, D., & Wong, K. (2013). Generating high spatiotemporal resolution land surface temperature for urban heat island monitoring. *IEEE Geoscience and Remote Sensing Letters*, *10*(5):1011-1015.

Kamal, A., Mahfouz, A., Sezer, N., Hassan, I. G., Wang, L. L., & Rahman, M. A. (2023). Investigation of urban heat island and climate change and their combined impact on building cooling demand in the hot and humid climate of Qatar. *Urban Climate*, *52*:101704.

https://doi.org/10.1016/J.UCLIM.2023.101704

Lafortezza, R., Carrus, G., Sanesi, G., & Davies, C. (2009). Benefits and well-being perceived by people visiting green spaces in periods of heat stress. *Urban Forestry and Urban Greening*, *8*(2):97-108.

Li, F., Yigitcanlar, T., Li, W., Nepal, M., Nguyen, K., & Dur, F. (2024). Understanding urban heat vulnerability: Scientometric analysis of five decades of research. *Urban Climate*, *56*:102035.

https://doi.org/10.1016/J.UCLIM.2024.102035

Li, X., Stringer, L. C., & Dallimer, M. (2022). The impacts of urbanisation and climate change on the urban thermal environment in Africa. *Climate*, *10*(11):164.

https://doi.org/10.3390/CLI10110164

Li, H., Jombach, S., Tian, G., Li, Y., & Meng, H. (2022). Characterizing temporal dynamics of urban heat Island in a rapidly expanding city: A 39 years study in Zhengzhou, China. *Land*, *11*(10):1838.

https://doi.org/10.3390/land11101838

Liu, L., Li, Q., Niu, Z., & Huo, X. (2024). Comparative study on information extraction of urban wetlands and its thermal environment using the SDGSAT-1 data. *International Journal of Digital Earth*, *17*(1):2310728.

https://doi.org/10.1080/17538947.2024.2310728

Mishra, P. K., Rai, A., & Rai, S. C. (2020). Land use and land cover change detection using geospatial techniques in the Sikkim Himalaya, India. *The Egyptian Journal of Remote Sensing and Space Science*, *23*(2):133-143.

Mohajerani, A., Bakaric, J., & Jeffrey-Bailey, T. (2017). The urban heat island effect, its causes, and mitigation, with reference to the thermal properties of asphalt concrete. *Journal of Environmental Management*, *197*:522-538.

Mu, B., Mayer, A. L., He, R., & Tian, G. (2016). Land use dynamics and policy implications in Central China: A case study of Zhengzhou. *Cities*, *58*:39-49.

https://doi.org/10.1016/J.CITIES.2016.05.012

National Bureau of Statistics. (2024). National Bureau of Statistics. Available from: https://www.nigerianstat.gov.ng [Last accessed on 2024 Oct 08].

Nieuwolt, S. (1966). The urban microclimate of Singapore. *Journal of Tropical Geography*, *22*:30-37.

Ogashawara, I., & Bastos, V. (2012) A quantitative approach for analyzing the relationship between urban heat Islands and land cover. *Remote Sensing*, *4*:3596-3618.

https://doi.org/10.3390/rs4113596

Oke, T. R. (1982). The energetic basis of the urban heat island. *Quarterly Journal of the Royal Meteorological Society, 108*(455):1-24.

Peng, J., Liu, Q., Xu, Z., Lyu, D., Du, Y., Qiao, R., *et al*. (2020). How to effectively mitigate urban heat island effect? A perspective of waterbody patch size threshold. *Landscape and Urban Planning*, *202*:103873.

Sarfo, I., Qiao, J., Effah, N. A. A., Yeboah, E., Alimo, P. K., Amara, D. B., *et al*. (2024). Advances in global land use systems development and sustainability: A bibliometric analysis. *Acta Scientiarum Polonorum. Formatio Circumiectus*, *23*(2):39-65.

https://doi.org/10.15576/ASP.FC/187717

Sarfo, I., Qiao, J., Yeboah, E., Okrah, A., El Rhadiouini, C., Osibo, B. K., *et al*. (2024). Causal effects and prediction of land use systems in rural landscapes: Evidence from Henan Province. *Acta Scientiarum Polonorum. Formatio Circumiectus*, *23*(3):27-56.

https://doi.org/10.15576/ASP.FC/190971

Taha, H., Akbari, H., Rosenfeld, A., & Huang, J. (1988). Residential cooling loads and the urban heat Island-the effects of albedo. *Building and Environment*, *23*(4):271-283.

Tesfamariam, S., Govindu, V., & Uncha, A. (2023). Spatio-temporal analysis of urban heat island (UHI) and its effect on urban ecology: The case of Mekelle city, Northern Ethiopia. *Heliyon*, *9*(2):e13098.

https://doi.org/10.1016/J.HELIYON.2023.E13098

Tian, L., Li, Y., Lu, J., & Wang, J. (2021). Review on urban heat island in china: Methods, its impact on buildings energy demand and mitigation strategies. *Sustainability (Switzerland)*, *13*(2):1-31.

https://doi.org/10.3390/SU13020762

United Nations Statistics Division. (2022). *Home-SDG Indicators*. Available from: https://unstats.un.org/sdgs [Last accessed on 2024 Dec 17].

Voogt, J. A., & Oke, T. R. (2003). Thermal remote sensing of urban climates. *Remote Sensing of Environment, 86*(3):370-384.

https://doi.org/10.1016/S0034-4257(03)00079-8

Vujovic, S., Haddad, B., Karaky, H., Sebaibi, N., & Boutouil, M. (2021). Urban heat island: Causes, consequences, and mitigation measures with emphasis on reflective and permeable pavements. *CivilEng, 2*(2):459-484.

https://doi.org/10.3390/CIVILENG2020026

Wang, H. (2024). The role of informal ruralization within China's rapid urbanization. *Nature Cities*, *1*(3):205-215.

https://doi.org/10.1038/s44284-024-00038-4

Wang, H., Qin, F., Xu, C., Li, B., Guo, L., & Wang, Z. (2021). Evaluating the suitability of urban development land with a Geodetector. *Ecological Indicators*, 123:107339.

Wu, X., Yang, Y., & Jiang, D. (2023). Dramatic increase in the probability of 2006-like compound dry and hot events over Southwest China under future global warming. *Weather and*

Climate Extremes, *41*:100592.

Yang, C., He, X., Wang, R., Yan, F., Yu, L., Bu, K., *et al.* (2017). The effect of urban green spaces on the urban thermal environment and its seasonal variations. *Forests*, *8*(5):153.

Zhang, C., Xiao, C., Li, S., Ren, Y., Zhang, S., Cai, X., *et al.* (2023). Analysis of the composite risk grade for multi extreme climate events in China in recent 60 years. *Climate*, *11*(9):191.

Zhang, Z., Zhang, M., Cao, C., Wang, W., Xiao, W., Xie, C., *et al.* (2020). A dataset of microclimate and radiation and energy fluxes from the Lake Taihu eddy flux network. *Earth System Science Data*, *12*(4):2635-2645.

Zhao, X., & Miao, C. (2022). Spatial-temporal changes and simulation of land use in metropolitan areas: A Case of the Zhengzhou Metropolitan Area, China. *International Journal of Environmental Research and Public Health*, *19*(21):14089.

https://doi.org/10.3390/IJERPH192114089

Zhao, W., Zhang, L., Li, X., Peng, L., Wang, P., Wang, Z., *et al.* (2022). Residents' preference for urban green space types and their ecological-social services in China. *Land*, *11*(12):2239.

Appendix

A1. Accuracy assessment

The accuracy assessment employed both the user's and producer's accuracy measures, in conjunction with the kappa coefficient, to analyze and validate the classification results. The kappa coefficient incorporated randomized and overall sampled points (100 samples for each respective year), facilitating a comprehensive evaluation of classification accuracy. Equation AI was used to calculate the accuracy assessment:

$$Accuracy\,assessment = \left(\frac{ASP}{TSP}\right)\times 100 \qquad \text{(AI)}$$

Where ASP = Average number of sample points that accurately fall on each required feature, and TSP = Total number of sample points generated.

1993:

TSP = 600

ASP = 556

$$Accuracy\,assessment = \left(\frac{556}{600}\right)\times 100$$

Accuracy rate (%) = 92.67

2003:

TSP = 600

ASP = 554

$$Accuracy\,assessment = \left(\frac{554}{600}\right)\times 100$$

Accuracy rate (%) = 92.33

2013:

TSP = 600

ASP = 557

$$Accuracy\,assessment = \left(\frac{557}{600}\right)\times 100$$

Accuracy rate (%) = 92.83

2023:

TSP = 600

ASP = 553

$$Accuracy\,assessment = \left(\frac{553}{600}\right)\times 100$$

Accuracy rate (%) = 92.17

Given the accuracy rates across the study period, the average accuracy rate for the entire duration is computed as follows:

$$Mean\ accuracy\ rate(\%) = \frac{(92.67+92.33+92.83+92.17)}{4}$$

Mean Accuracy rate (%) = 92.50

A2. The influence of land use and land cover change on urban heat island decadal variation during extreme hot and dry events

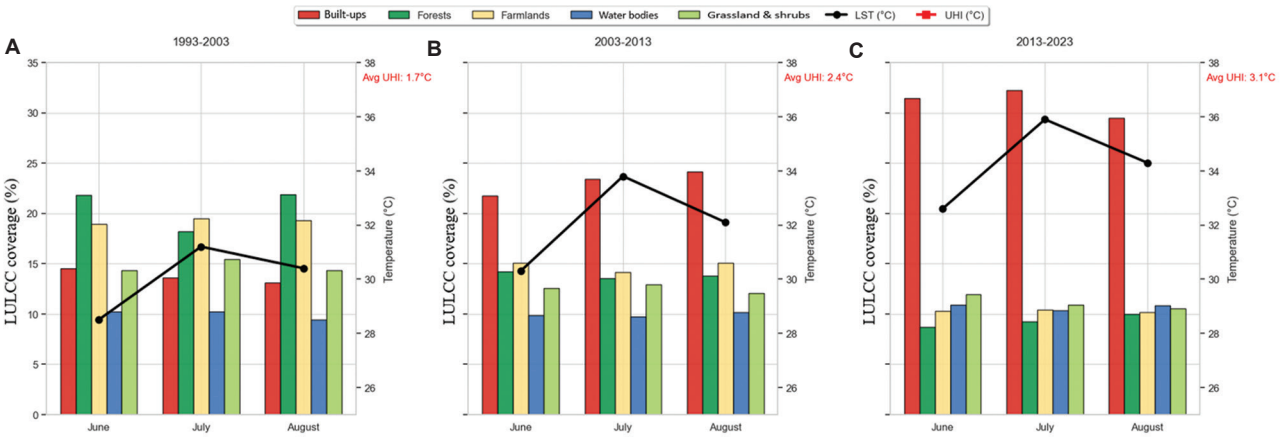

Figure A1. The effects of land use and land cover change on land surface temperature and urban heat island during extreme hot and dry events in Zhengzhou city, Henan, China, over the past 30 years (1993 – 2023). (A) 1993 – 2003; (B) 2003 – 2013; (C) 2013 – 2023
Source: Graphs by the authors